Supporting Information

Swift et al. 10.1073/pnas.1018280108

SI Methods

Experimental Animals, Cells, and Expression Vectors. Mice expressing EGFP or tomato reporter genes in dopamine 2 receptor (D2R)- and D1R-positive neurons (D1tom/D2gfp mice), respectively, were obtained by breeding drd2-EGFP mice with drd1a-tdTomato (using a standard two-step breeding procedure) (1). drd2-EGFP bac transgenic mice were obtained from gensat, and drd1a-tdTomato bac transgenic mice were described previously (2). The Université Laval Institutional Animal Care Committee approved all experimental procedures involving animals in line with guidelines from the Canadian Council on Animal Care.

Antibodies and Chemicals. Antiphospho-Akt (Ser473), antitotal–extracellular-regulated kinase (Erk) 1/2, and antiphospho-ERK1/2 (Thr202/Tyr204) were purchased from Cell Signaling Technology. Antitotal-Akt monoclonal antibodies were obtained from Biosources. Monoclonal mouse anti-GFP antibodies were from Santa Cruz Biotechnology, and antiactin clone c4 monoclonal antibodies were from Chemicon/Milipore. The antiphospho-EGF receptor (EGFR; Tyr1068) was from epitomics, and the anti-TrkB extracellular epitope antibody was from R&D Systems. EGF and brain-derived neurotrophic factor (BDNF) were obtained from Prospec.

Primary Neuron Cultures. Striata were dissected from 1- to 3-day-old D1tom/D2gfp double transgenic pups. Briefly, cells were plated on 18-mm Aclar* (22C 5 mL) coverslips (P5000HS; Honeywell) coated with 100 μg/mL poly-D-lysine at a concentration of 2×10^6 cells/mL. After 24 h in culture, cells were rinsed in neurobasal media and placed in complete growth media. After 15 days in culture, the medium was removed and replaced by serum-free growth media or media containing BDNF, apomorphine (Apo), or AG1478. Neurons were maintained in complete neurobasal growth media that was composed of neurobasal and B27 supplemented with 0.5 mM L-glutamax (Invitrogen), 5% FBS, and 50 U/mL;50 μg/mL penicillin/streptomycin.

Transfection and Cell Culture. Chinese hamster ovary (CHO-k1) cells stably expressing ~600,000 EGFR-GFP receptors per cell are described elsewhere (3). Cells were grown to 70–85% confluence and transiently transfected using Lipofectamine LTX reagent (Invitrogen). GPCR constructs included angiotensin 1a receptor (At1aR), D2R, D1R, β_2-adrenergic receptor (β_2AR), and neurokinin-1 receptor (NK-1r). In some cases, an Rab5 S34N dominant negative mutant (4) was cotransfected to prevent EGFR internalization (5). All experiments were done 48 h post-transfection.

CHO-K1 cells were maintained in DMEM containing 1,000 mg/mL D-glucose, 10% heat-inactivated FBS, 0.1 mM nonessential amino acids, 4 mM L-glutamine, 100 U/mL penicillin, 0.1 mg/mL streptomycin (Invitrogen), and 400 μg/mL Geneticin (Invitrogen).

Cell Fixation. Twenty-four hours after transfection, cells were lifted using 0.25% trypsin solution (Invitrogen), transferred to MatTek dishes coated with 2 μg/mL fibronectin, and grown for an additional 24 h. After 16 h serum starvation, transfected cells were stimulated through the addition of appropriate ligands. Cells were fixed using a 4% paraformaldehyde for 10 min and rinsed two times with PBS. After the fixation procedure, cells were kept moist through the addition of 1 mL PBS and were stored at 4 °C before imaging.

For immunodetection, antibodies were diluted in 2% normal goat serum in PBS. Monoclonal anti-mouse TrkB antibody was diluted at 1:20 and incubated overnight at 4 °C. Coverslips were rinsed three times with PBS. Incubation with the secondary antibody was performed for 1 h at room temperature (alexa fluor 647 goat anti-rat; Invitrogen).

Immunoblots. Cells were grown on 100-mm Petri dishes and serum-starved for 12 h before stimulation with EGF (1 μM × 5 min at 37 °C) with or without preincubation in AG1478 (200 μM × 15 min at 37 °C). Cells were rinsed two times in ice-cold PBS, centrifuged, frozen in liquid nitrogen, and stored at −80 °C before protein extraction. Frozen pellets were lysed in 125 μL boiling 1% SDS and sonicated as described (6). Protein concentration in extracts was measured using a DC protein assay (Bio-Rad). Western blots were made using 25 μg total protein and were incubated with primary antibodies as described (7). Immune complexes were revealed using appropriate IR dye-labeled secondary antibodies from Licor and detected using an Odyssey Imager (Licor).

Microscopy. All images were obtained using an Olympus FV300 scan head and an Olympus IX71 inverted confocal laser scanning microscope (Olympus America) with a 60× plan-apochromactic oil immersion objective (numerical aperture = 1.4). Sample excitation was achieved using 1% of a 40-mW, 488-nm line of an argon laser and dichroic filter FV-FCB GR 488/543/633. Emission was collected through the same objective and dichroic filter and passed through a BA510IF long-pass emission filter. Photomultiplier tubes (PMT) voltages in the detection channel were set to 600 V, ensuring no saturation and that most pixel intensities were in the linear range of the detector (i.e., no pixel saturation). Pinhole 2 was used corresponding to a point-spread function (PSF) in the x and y dimensions of 0.2 μm. The pixel resolution for images of the CHO-k1 EGFR-GPCR cells was 0.092 μm/pixel, and the pixel resolution for images of TrkB in primary cell culture neurons was 0.058 μm/pixel. All images were 1,024 × 1,024 pixels in size collected using the slowest scan speed available corresponding to a pixel dwell time of 9.1 μs/pixel. Confocal laser-scanning microscopy (CLSM) settings were kept constant for all samples to ensure that comparisons could be made between samples.

Spatial Intensity Distribution Analysis. The fitting function for a system with density of N particles is (Eq. S1)

$$H(\varepsilon, N; k) = \sum_n \rho^n(\varepsilon; k) \cdot poi(n, N) \quad \text{[S1]}$$

with (Eq. S2)

$$\rho^0(\varepsilon; k) = \delta_{k,0}, \quad \text{[S2]}$$

where (Eq. S3)

$$\rho^n(\varepsilon; k) = \rho^1(\varepsilon; k) \otimes \rho^{n-1}(\varepsilon; k) \quad \text{[S3]}$$

with (Eq. S4)

$$\rho^1(\varepsilon; k) = \int \delta(\varepsilon \cdot I(\mathbf{r}) - k) d\mathbf{r}. \quad \text{[S4]}$$

$I(r)$ is the illumination intensity profile of the excitation laser, ε represents the quantal brightness of a single fluorescent particle,

and k is the probability of observing an intensity of light (assumed to be proportional to the number of photons emitted). H is normalized over all intensity values so that the integral over k equals one. A constant factor, A, is introduced, which is the number of pixels in a subregion of the image where the fluorescent particles are distributed. This allows for the fit of an image intensity histogram to be performed. Three parameters are fit in Eqs. **S1** and **S2**: the number of pixels (A), the fluorescent particle density (N particles per laser beam effective focal volume), and the quantal brightness (ε intensity units in IU per unit of pixel integration time). Because the images are collected with CLSM, the fluorescence intensity is measured using PMTs, and the number of collected photoelectrons is a function of the polarization voltage.

If dimers are present in the sample, they will yield quantal brightness of 2ε. When the monomer and dimer populations are mixed within the same region in space, the total histogram becomes the convolution of the two individual distributions (Eq. **S5**):

$$H(\varepsilon_1, N_1, \varepsilon_2, N_2, A; k) = A \cdot H(\varepsilon_1, N_1; k) \otimes H(\varepsilon_2, N_2; k). \quad \textbf{[S5]}$$

To improve the fitting of our data, the signal for monomeric GFP was obtained by transfecting a membrane-targeted monomeric GFP construct (8) into CHO-k1 cells containing no EGFR-GFP. The cells were otherwise cultured and fixed using the same procedures as outlined above for the EGFR-GFP–containing cells. To obtain a value for the monomeric signal of the antibody-labeled TrkB receptor, samples were treated with AG1478 to prevent TrkB dimerization. These critical measurements were determined before each experiment and incorporated into the fitting model. To obtain accurate results, noise characteristics of the detector also had to be studied and taken into account in the analysis (see ref. 9 for complete analysis).

For the present studies, two to three regions of interest (~100–200 beam areas) were analyzed per cell. This was done to guarantee that we only analyze areas that seem to be homogenous (i.e., no structural features including adhesions). To ensure that increased dimer density resulting from transactivation was not spatially limited to only a few regions of the cells, we produced a dimer density map illustrating distribution of EGFR dimers both for nonstimulated cells and as a function of transactivation. In Fig. S4, a square region of 32 × 32 pixels (pi) [corresponding to 69 beam areas (BAs)] was scanned throughout the image, and spatial intensity distribution analysis (SpIDA) (Eqs. **S3** and **S4**) was applied individually to each of the regions. The densities of monomeric, dimeric, and total EGFRs were obtained for each small regions, and 2D maps of the dimer density, total EGFR density, and ratio of dimers over total oligomer [D/(M + D)] are shown. This type of analysis is shown for both control non-stimulated cells and stimulated cells (Iso = 500 nM).

From the resulting maps, we determine that EGFR dimerization from transactivation is not limited to certain areas within the cell but that occurs across the whole basal membrane of the cells. Importantly, the average dimer density, total protein density, and percent dimer density agree with values obtained from averaging six individual titrations.

Fluorescence Lifetime Imaging/Förster Resonance Energy Transfer Measurements. For fluorescence lifetime imaging (FLIM)/Förster resonance energy transfer (FRET) analysis of EGFR dimerization, stable CHO-k1 cells expressing EGFR-GFP were cotransfected with the EGFR-mCherry construct alone or in combination with GPCR expression plasmids, and they were cultured as described previously. Cells were then plated onto glass coverslips, stimulated, fixed with 4% paraformaldehyde, and mounted in Prolong Gold (Invitrogen). For FLIM, samples were illuminated with a Chameleon Ultra IR laser (Coherent) at 80 MHz repetition rate tuned at 900 nm for GFP two-photon excitation.

The acquisition of fluorescence lifetimes was synchronized by a time-correlated single photon-counting (TCSPC) module (SPC-830; Becker and Hickl). Measurements were performed on a Zeiss LSM 510 microscope using a 63× oil immersion objective. Fluorescence emission was detected with a cooled high-speed PMT detector head (PMC-100–1; Becker and Hickl) between 505 and 545 nm by means of a GFP emission filter (HQ525/40m; Chroma). The following parameters were kept constant for all acquired images: pixel size (100 nm and 512 × 512 pixels), pixel dwell time (1.60 μs), laser excitation intensity (6%), and FLIM acquisition time (60 s/image). Using these parameters, no photobleaching of either GFP or mCherry was observed. Reference green and red images in confocal mode were also recorded for each FLIM image (GFP excitation at 488 nm and mCherry excitation at 543 nm).

Fluorescence lifetime images were analyzed with SPCimage (Becker and Hickl). For all images, a binning factor of 10 pixels was used to have sufficient photons in the regions of interest and then, reduce the error on the calculated lifetime. For the same concerns, a threshold was applied to avoid lifetime calculations in low-intensity pixels (40 photons at the peak was the minimal threshold used). Furthermore, the same calculated instrumental response function was used for all images. Because the signal is contaminated with uninteracting proteins (because of unassembled EGFRs, mCherry-tagged dimers, or dimers with one labeled EGFR), the single exponential model was a better fit, even in high FRET regions. Accordingly, the FLIM images were all analyzed with a single exponential model. For each cell, the lifetimes of all pixels were extracted in an intensity-weighted lifetime distribution histogram. These distributions were then analyzed in Matlab to normalize them and calculate a mean lifetime for each cell.

1. Beaulieu JM, Julien JP (2003) Peripherin-mediated death of motor neurons rescued by overexpression of neurofilament NF-H proteins. *J Neurochem* 85:248–256.
2. Shuen JA, Chen M, Gloss B, Calakos N (2008) Drd1a-tdTomato BAC transgenic mice for simultaneous visualization of medium spiny neurons in the direct and indirect pathways of the basal ganglia. *J Neurosci* 28:2681–2685.
3. Brock R, Hamelers IH, Jovin TM (1999) Comparison of fixation protocols for adherent cultured cells applied to a GFP fusion protein of the epidermal growth factor receptor. *Cytometry* 35:353–362.
4. Seachrist JL, Anborgh PH, Ferguson SS (2000) beta 2-adrenergic receptor internalization, endosomal sorting, and plasma membrane recycling are regulated by rab GTPases. *J Biol Chem* 275:27221–27228.
5. Barbieri MA, et al. (2000) Epidermal growth factor and membrane trafficking. EGF receptor activation of endocytosis requires Rab5a. *J Cell Biol* 151:539–550.
6. Beaulieu JM, et al. (2008) Role of GSK3 beta in behavioral abnormalities induced by serotonin deficiency. *Proc Natl Acad Sci USA* 105:1333–1338.
7. Beaulieu JM, Sotnikova TD, Gainetdinov RR, Caron MG (2006) Paradoxical striatal cellular signaling responses to psychostimulants in hyperactive mice. *J Biol Chem* 281: 32072–32080.
8. Hudmon A, et al. (2005) A mechanism for Ca2+/calmodulin-dependent protein kinase II clustering at synaptic and nonsynaptic sites based on self-association. *J Neurosci* 25: 6971–6983.
9. Godin AG, et al. (2011) Revealing protein oligomerization and densities in situ using spatial intensity distribution analysis. *Proc Natl Acad Sci USA*, 10.1073/pnas. 1018658108.

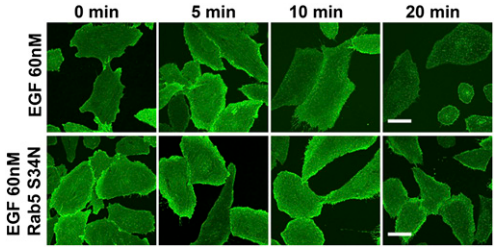

Fig. S1. Sample CLSM images of the basal membrane of CHO-k1 cells expressing EGFR-GFP receptors at 0, 5, 10, and 20 min after stimulation with EGF (60 nM) with and without Rab5 S34N mutant. (Scale bar, 20 μm.)

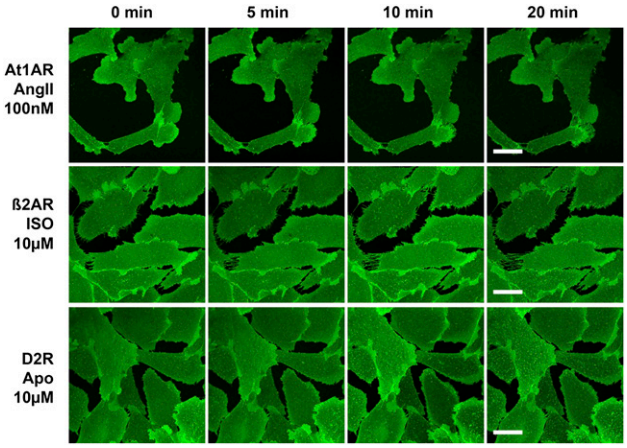

Fig. S2. CLSM images of the basal membrane of CHO-k1 cells expressing EGFR-GFP and At1aR, β_2AR, and D2R receptors at 0, 5, 10, and 20 min after stimulation with Angiotensin II (100 nM), Iso (10 μM), and Apo (10 μM), respectively. (Scale bar, 20 μm.)

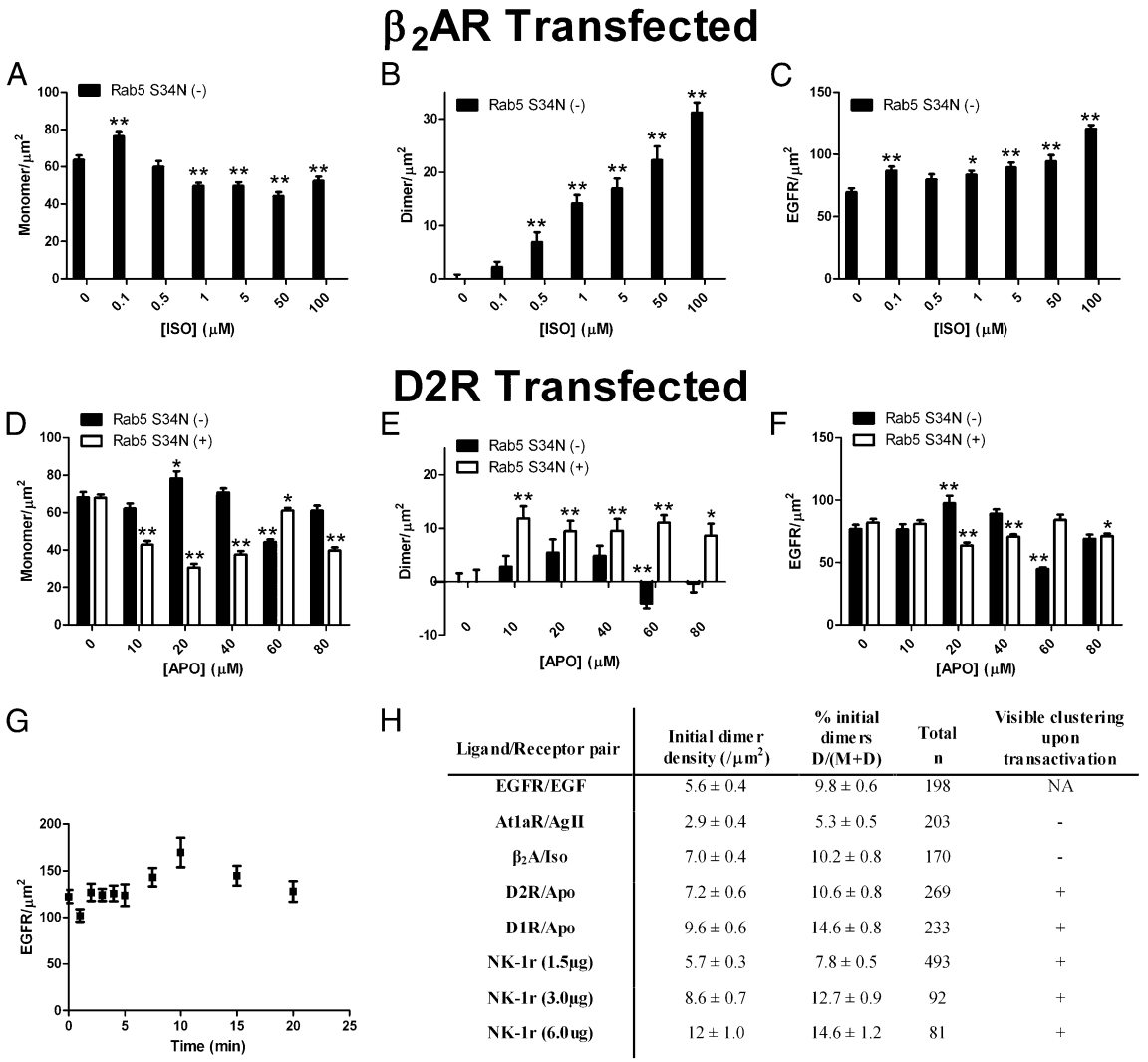

G

H

Ligand/Receptor pair	Initial dimer density (/μm^2)	% initial dimers D/(M+D)	Total n	Visible clustering upon transactivation
EGFR/EGF	5.6 ± 0.4	9.8 ± 0.6	198	NA
At1aR/AgII	2.9 ± 0.4	5.3 ± 0.5	203	-
β_2A/Iso	7.0 ± 0.4	10.2 ± 0.8	170	-
D2R/Apo	7.2 ± 0.6	10.6 ± 0.8	269	+
D1R/Apo	9.6 ± 0.6	14.6 ± 0.8	233	+
NK-1r (1.5μg)	5.7 ± 0.3	7.8 ± 0.5	493	+
NK-1r (3.0μg)	8.6 ± 0.7	12.7 ± 0.9	92	+
NK-1r (6.0ug)	12 ± 1.0	14.6 ± 1.2	81	+

Fig. S3. Dimer and total particle density plots describing internalization and effect of Rab5 S34N. (*A–C*) SpIDA analysis of EGFR monomer, dimer, and total particle densities at 1 min poststimulation resulting from β_2AR stimulation (n = 25 cells/bar). (*D–F*) SpIDA analysis of EGFR monomer, dimer, and total particle densities after stimulation of D2R with Apo with (n = 32 cells/bar) and without Rab5 S34N (n = 17 cells/bar). In all cases, the basal dimer density has been subtracted from the subsequent concentrations. Values of dimer densities that are lower than initial basal levels are represented here as negative numbers. (*G*) Total EGFR surface protein density as a function of time in cells expressing β_2AR are activated with 10 μm Iso (n = 18 cells/point from one experiment). All data are mean ± SEM. *$P \leq 0.05$, **$P \leq 0.01$ compared with respective unstimulated conditions (Dunnett's multiple comparison test).

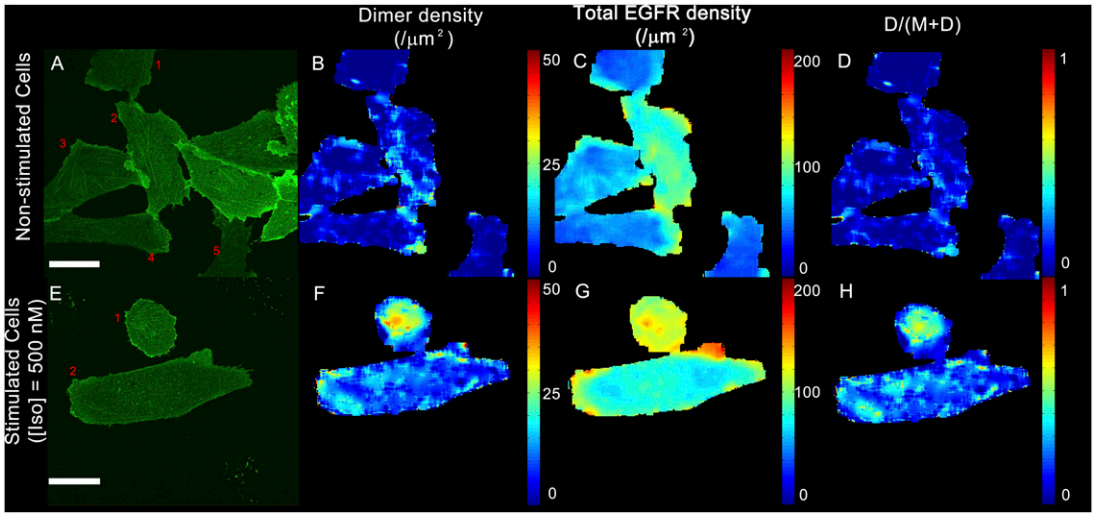

Fig. S4. Representative CLSM images of the basal membrane of CHO-k1 cells expressing EGFR-GFP (*A*) and co-expressing β_2AR (*E*), after stimulation with 500 nM Iso. For each image, an (*x,y*) density map of the dimer density (*B* and *F*), the total EGFR density (*C* and *G*), and percent dimers (*D* and *H*) were generated for five cells (numbered 1 to 5 in *A*) and two cells (numbered 1 and 2 in *E*). Each point in the map results from the analysis of a 32 × 32 square pixel region that corresponds to 69 BAs. The squared region was scanned throughout the whole image with a step size of four pixels. For the nonstimulated cell (*A*), the average dimer density was found to be 4.1 ± 2.8/μm^2 (*B*), the mean total particle density was found to be 65 ± 10/μm^2 (*C*), and the percent EGFR dimers was 6.4 ± 4.4% (*D*). For the cell expressing β_2AR stimulated with Iso (*E*), the average dimer density was found to be 12.5 ± 5.3/μm^2 (*F*), the mean total particle density was 70 ± 11/μm^2 (*G*), and the percent EGFR dimers was 23 ± 9% (*H*). (Scale bar: 20 μm.)

Table S1. D_{50} for EGFR-GFP dimerization measured by SpIDA after direct stimulation by EGF or stimulation of diverse GPCR/ligand pairs in CHO-k1 cells

Ligand/receptor pair	D_{50} (nM; EGFR)	$FRET_{50}$ (nM; EGFR)	K_d (nM; published)	References
EGFR/EGF	89 ± 8	30 ± 20	0.07–6	1 and 2
At1aR/AngII	3.0 ± 1.0	12 ± 6	1.0–8.0	3–15
β2AR (1.5 μg)/Iso	500 ± 40	NA	240–460	6 and 7
β2AR (6.0 μg)/Iso	200 ± 166	NA	240–460	6 and 7
D2R/Apo	51 ± 38	NA	1.0–63	8–10
D1R/Apo	9.0 ± 6.0	NA	9.0–400	11–13
NK-1r (1.5 μg)/SubP	0.5 ± 0.3	NA	0.35–2.0	14 and 15
NK-1r (6.0 μg)/SubP	1.1 ± 0.8	NA	0.35–2.0	14 and 15
NK-1r/NKA	50 ± 20	NA	0.5–650	16–18

AgII, angiotensin II; Iso, isoproterenol; NA, not assessed; Apo, apomorphine; SupP, substance P; NKA, neurokinin A. The range of K_d values given reflects the large variability in reported K_d values in the literature, typically from competition binding assays.

1. Holbrook MR, Slakey LL, Gross DJ (2000) Thermodynamic mixing of molecular states of the epidermal growth factor receptor modulates macroscopic ligand binding affinity. *Biochem J* 352(Pt 1):99–108.
2. Zhou M, et al. (1993) Real-time measurements of kinetics of Egf binding to soluble Egf receptor monomers and dimers support the dimerization model for receptor activation. *Biochemistry* 32(32):8193–8198.
3. Chiu AT, et al. (1993) Characterization of angiotensin AT1A receptor isoform by its ligand binding signature. *Regul Pept* 44(2):141–147.
4. Vanderheyden PML, Fierens FLP, De Backer JP, Fraeyman N, Vauquelin G (1999) Distinction between surmountable and insurmountable selective AT(1) receptor antagonists by use of CHO-K1 cells expressing human angiotensin II AT(1) receptors. *Br J Pharmacol* 126(4):1057–1065.
5. Georgsson J, et al. (2005) Angiotensin II pseudopeptides containing 1,3,5-trisubstituted benzene scaffolds with high AT(2) receptor affinity. *J Med Chem* 48(21):6620–6631.
6. Liang W, Hoang Q, Clark RB, Fishman PH (2008) Accelerated dephosphorylation of the beta2-adrenergic receptor by mutation of the C-terminal lysines: Effects on ubiquitination, intracellular trafficking, and degradation. *Biochemistry* 47(45):11750–11762.
7. Hoffmann C, Leitz MR, Oberdorf-Maass S, Lohse MJ, Klotz KN (2004) Comparative pharmacology of human beta-adrenergic receptor subtypes: Characterization of stably transfected receptors in CHO cells. *Naunyn-Schmiedebergs Arch Pharmacol* 369(2):151–159.
8. Freedman SB, et al. (1994) Expression and pharmacological characterization of the human D3 dopamine receptor. *J Pharmacol Exp Ther* 268(1):417–426.
9. Sautel F, et al. (1995) A functional test Identifies dopamine agonists selective for D3 versus D2 receptors. *Neuroreport* 6(2):329–332.
10. Martres MP, Sokoloff P, Schwartz JC (1984) Dopaminergic binding-sites in rat striatal slices and the action of guanyl nucleotides. *Naunyn-Schmiedebergs Arch Pharmacol* 325(2):116–123.
11. Toll L, et al. (1998) Standard binding and functional assays related to medications development division testing for potential cocaine and opiate narcotic treatment medications. *NIDA Res Monogr* 178:440–466.
12. Seeman P, Guan HC (1987) Dopamine-D1 and dopamine-D2 receptors are sensitive to the cationic form of apomorphine. *Mol Pharmacol* 32(6):760–763.
13. Acerbo MJ, Vyboh P, Kost'al L, Kubikova L, Delius JD (2005) Repeated apomorphine administration alters dopamine D1 and D2 receptor densities in pigeon basal telencephalon. *Exp Brain Res* 160(4):533–537.
14. Cascieri MA, et al. (1992) Characterization of the binding of a potent, selective, radioiodinated antagonist to the human neurokinin-1 receptor. *Mol Pharmacol* 42(3):458–463.
15. Takeda Y, et al. (1992) Ligand-binding kinetics of substance-P and neurokinin-a receptors stably expressed in Chinese-hamster ovary cells and evidence for differential stimulation of inositol 1,4,5-trisphosphate and cyclic-amp 2nd-messenger responses. *J Neurochem* 59(2):740–745.
16. Sarau HM, et al. (1997) Nonpeptide tachykinin receptor antagonists. I. Pharmacological and pharmacokinetic characterization of SB 223412, a novel, potent and selective neurokinin-3 receptor antagonist. *J Pharmacol Exp Ther* 281(3):1303–1311.
17. Gether U, et al. (1993) 2 Nonpeptide tachykinin antagonists act through epitopes on corresponding segments of the Nk1 and Nk2 receptors. *Proc Natl Acad Sci USA* 90(13):6194–6198.
18. Hastrup H, Schwartz TW (1996) Septide and neurokinin A are high-affinity ligands on the NK-1 receptor: Evidence from homologous versus heterologous binding analysis. *FEBS Lett* 399(3):264–266.